

*Scientific Project*

OPTICAL OPTIMIZATION OF  
NANOPATTERNED PEROVSKITE SOLAR CELLS

Rui de Andrade e Costa, 106197

Supervisors:  
Miguel Alexandre, NOVA FCT  
Luís Viseu Melo, IST

June 27, 2025

## Abstract

This work presents an optical optimization study of perovskite solar cells (PSCs) incorporating nanopatterned structures to enhance light trapping and absorption. Using Ansys Lumerical FDTD Solutions,  $\text{CH}_3\text{NH}_3\text{PbI}_3$ -based devices were simulated under both terrestrial (AM1.5G) and extraterrestrial (AM0) solar spectra to evaluate optical performance. The study employed a particle swarm optimization (PSO) algorithm to determine the optimal nanophotonic configuration maximizing the short-circuit current density ( $J_{PH}$ ). Comparative analysis showed an 18.6% increase in  $J_{PH}$  due to nanopatterning under AM1.5G, and a 19.6% increase under AM0. Detailed convergence tests validated numerical stability, and parametric sweeps highlighted the sensitivity of device performance to geometry variations. Additionally, angular and polarization effects on absorption were examined to assess real-world robustness. The findings demonstrate the importance of nanophotonic design in optimizing PSCs, especially for space applications, while also identifying future steps for integrating optical and electrical modeling.

## I. INTRODUCTION

With silicon solar cells close to reaching their intrinsic efficiency limit of 29% for single-junction cells, measuring records of 26.7%, [1] efforts at further advancing photovoltaic efficiency have turned towards alternative materials and light management ideas. Perhaps most strikingly, incorporation of nanostructures on the sub-wavelength scale has been found to maximize light trapping and absorption, and consequently the photocurrent, without significantly increasing material consumption.

Parallel to these advancements, perovskite solar cells (PSCs) are positioning themselves as a serious contender in the photovoltaic market, with efficiencies in the lab of up to 25%. [2] Among the several perovskite materials, methylammonium lead iodide  $\text{CH}_3\text{NH}_3\text{PbI}_3$  remains one of the most widely studied due to its excellent optoelectronic characteristics, easy fabrication, and high absorption coefficient. But it suffers from two critical issues: inherent instability, especially when exposed to environmental stresses such as heat and moisture [3], and toxicity due to the presence of lead [4].

Still, optical analysis is especially crucial in methylammonium lead iodide solar cell design since it enables a precise comprehension of light behavior in each layer within the device. By simulating absorption, interference, and scattering effects in the entire stack, the structures that maximize photocurrent while minimizing material demands can be established. This process illustrates how performance is a function of layer thickness, material stack, and nanostructure geometry decisions—factors unknown from electrical modeling. Even in materials with known issues such as  $\text{CH}_3\text{NH}_3\text{PbI}_3$ , optical analysis remains required for exploring the design space and guiding experimental effort to efficient and physically reasonable configurations.

This project explores a hybrid optimization method, combining perovskite active layers with nanostructured optical components to achieve maximum light trapping and absorption. The study uses *Ansys Lumerical FDTD Solutions* for calculation of the optical performance of nanopatterned  $\text{CH}_3\text{NH}_3\text{PbI}_3$ -based solar cells under Earth's AM1.5G and space's AM0 solar spectra. Ultimately, this study determined the nano-photonic configuration that leads to the best optical absorption, and how this performance changes with different spectral conditions.

### A. Structure of the Solar Cell

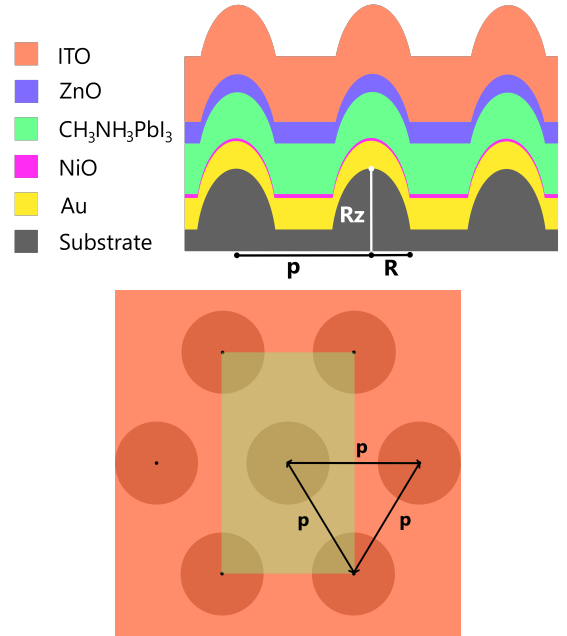


Figure 1: Sketches of the cell structure (not to scale) from a cross-section and top view.  $R$ ,  $R_z$  and  $p$  are the optimization parameters. The lime green area in the top view represents the simulation zone.

The solar cells modeled in this work are based on the configurations studied in [5]. This cell consists of a gold (Au) rear metal contact, with a nickel oxide (NiO) electron transport layer (ETL), a zinc oxide (ZnO) hole transport layer (HTL), an indium tin oxide (ITO) front electrode and, as stated before, a methylammonium lead iodide ( $\text{CH}_3\text{NH}_3\text{PbI}_3$ ) active layer. Such a layer structure can be fabricated via wet-coating onto a patterned substrate, in order to obtain the spheroidal structures studied. This makes it so they aren't unrealistic to later recreate in a lab or industrial setting. The structure presented in [6] is replicated in figure 1.

## B. Relevant Quantities

To evaluate and design the optical performance of the simulated nanostructured perovskite solar cells in this study, several different quantities were computed. These depend on the underlying electromagnetic field-matter interaction and are the link between raw optical simulation results and performance-critical magnitudes such as photocurrent. The following definitions allow for spatially and spectrally resolved measurement of absorption, generation, and current density, and thus form the foundation of this work. [5]

$$P_{\text{ABS}} = \frac{1}{2} \omega \epsilon'' |\mathbf{E}|^2 \quad (1)$$

This is the volumetric absorption of optical power of a material, derived from Maxwell's equations expressed in the frequency domain. Here,  $\omega$  is angular frequency,  $\epsilon''$  is imaginary part of dielectric permittivity, and  $|\mathbf{E}|^2$  is local electric field. This is used to calculate how light is absorbed spatially in terms of various materials in the cell. Integrating this power over the perovskite domain makes it possible to estimate how well the nanophotonic structure traps light.

$$\text{Abs}(\lambda) = \int p_{\text{ABS}}(\lambda) dV \quad (2)$$

This describes the wavelength-dependent total absorption in the perovskite film through integration of power density absorbed over the film volume. It shows the fraction of light incident at each wavelength that is steered toward absorption in the active layer, as compared to parasitic losses in inactive layers (e.g., TCO, ETL, HTL). The  $\text{Abs}(\lambda)$  function is used directly in calculation of  $J_{\text{PH}}$ , giving spectrally-resolved insight into how nanostructures impact device efficiency across the solar spectrum.

$$J_{\text{PH}} = e \int \frac{\lambda}{hc} \text{Abs}(\lambda) I_{\text{AM1.5G}}(\lambda) d\lambda \quad (3)$$

This equation calculates the maximum possible short-circuit current density achieved at nominal solar irradiation (AM1.5G) assuming perfect internal quantum efficiency (100% of photons absorbed result in collected carriers). It is an upper bound on the actual current a device is able to generate and as such, it is a useful figure of merit for optimizing optical designs before electrical effects (e.g., recombination). Here, it is used as the objective function in the optimization routine to guide nanostructure geometry changes to the optimal with respect to maximizing light absorption in the perovskite layer in particular. Altering this for the AM0 spectrum simply implies subbing it in for  $I_{\text{AM1.5G}}$ .

$$G = \int g(\omega) d\omega \quad (4)$$

This expression gives the overall rate of electron-hole pair generation (units of  $m^{-3}s^{-1}$ ) by integrating the spectral generation rate  $g(\omega)$ , which is itself derived from absorbed power divided by photon energy.  $G$  is of crucial relevance in transitioning from optical to electrical simulations because it is the source term in the continuity equations used in drift-diffusion electrical models.

## C. Methods and Software Used

To calculate these values, Ansys Lumerical FDTD (Finite-Difference Time-Domain) [7] solvers were utilized. The FDTD method strictly solves Maxwell's equations in the time domain, which allows for the correct determination of light absorption, scattering, and field distributions within the cell structures [8]. By utilizing Lumerical's advanced parametric sweep and optimization tools, design parameters such as grating period, thickness, and nanostructure geometry can be systematically changed to maximize light trapping and absorption efficiency. Additionally, its post-processing features facilitated the evaluation of key metrics like the ones mentioned before, and, as such, ultimate efficiency.

Additionally, the models for the layer materials were derived from experimental data. Since there isn't any current dataset that represents a technological standard, this can generate differences in results.

To properly evaluate  $J_{\text{PH}}$  for the patterned perovskite layer, Lumerical's power absorption monitor

had to be altered to only use data from the specific material of the active layer. Furthermore, the absorption calculation monitors were altered for the AM0 spectrum using data from [9]. This was done by altering the solar spectrum wavelength vector inside the  $P_{abs}$  monitor analysis script.

Finally, throughout simulations, 251 frequency points were considered, along with 1000 time steps. The light source was considered to be a plane wave with wavelengths ranging from  $300\text{nm}$  to  $1\mu\text{m}$ . For all sections, PML boundary conditions were used for  $z_{max}$  and  $z_{min}$  to avoid reflections. Other boundaries were consistent across every section except section VI, those being  $x_{max}$  and  $x_{min}$  set to anti-symmetric, and  $y_{max}$  and  $y_{min}$  set to symmetric, since the cell structure is infinitely periodic. In the case of section VI, where the angular and polarization dependence of the photocurrent was studied, Bloch boundary conditions were instead applied along the  $x$  and  $y$  directions. This change was necessary to correctly model oblique incidence on a periodic structure, as Bloch boundaries allow the fields to acquire a phase shift across the boundaries that matches the in-plane wavevector of the incident light.

## II. MODEL CREATION AND VALIDATION

To first validate that the proposed model works, the cell structure was manually recreated in Lumerical, along with the analogous planar structure. For this, simulation parameters that resulted from an optimization performed in [5] and present in Table I were utilized.

Table I: Layer thicknesses and geometrical parameters

Parameter	Value
$h_{\text{ITO}}$	350 nm
$h_{\text{ZnO}}$	100 nm
$h_{\text{NiO}}$	10 nm (spheroids), 50 nm (planar)
$h_{\text{CH}_3\text{NH}_3\text{PbI}_3}$	300 nm
$h_{\text{Au}}$	200 nm
$R$	254.2 nm
$R_z$	662.8 nm
$p$	508.4 nm

Figure 2 confirms that the structure was properly implemented, as the individual layers and their corresponding thicknesses are clearly distinguishable

through their refractive indexes at two critical regions within the simulation area.

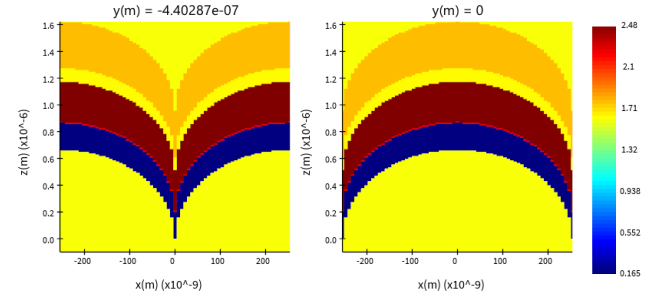


Figure 2: Refractive index cross-section at the edge and center of the simulation zone, used to verify the sound creation of the cell structure.

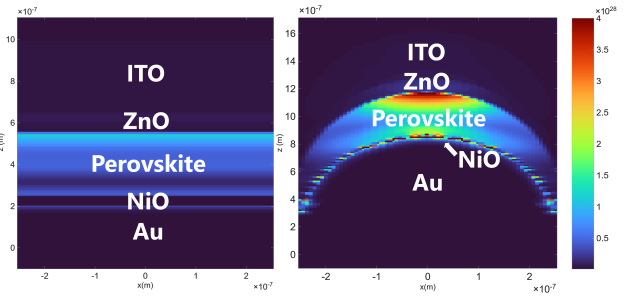


Figure 3: Rate of electron-hole pair generation for the nanopatterned cell and for the planar cell structures, in an xz cross-section at  $y=0$ .

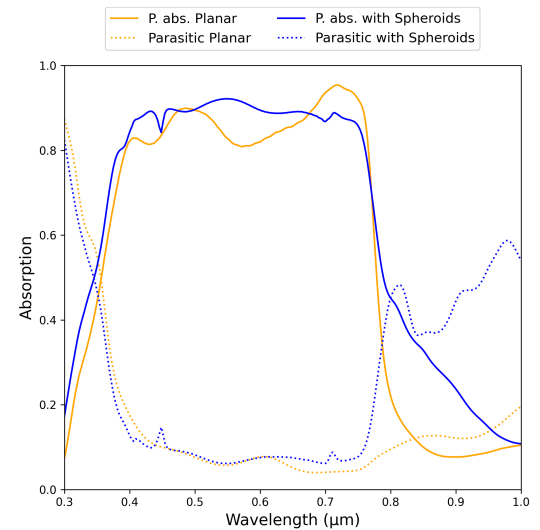


Figure 4: Light absorption spectra of the cells with and without spheroidal structures. Parasitic absorption represents the absorption of the non-perovskite layers.

The absorption per wavelength for the perovskite layer was calculated using the  $P_{abs}$  monitor and the

absorption for the whole cell was calculated using a solar power monitor. Subtracting one from the other yields the parasitic absorption, as can be seen in figure 4. Furthermore, the rate of electron-hole pair generation was obtained and is similar to the one presented in [6], and the  $J_{PH}$  and was obtained and compared to the reference material in table II.

Table II:  $J_{PH}$  comparison between reference values (Ref.) and current model (Rec.) for planar and patterned (Sp.) structures.

	Ref. [5]	Rec.
Planar $J_{PH}$ ( $mA/cm^2$ )	22.6	22.6
Sp. $J_{PH}$ ( $mA/cm^2$ )	27.6	26.8
% Increase	22.1	18.6

These small differences in the  $J_{ph}$  of the patterned cell are because of variations in material fit, simulation parameter variations, and numerical effects such as mesh discretization. Even if the same structural parameters are used, slightly different interpolations of refractive indices of materials over the wavelength range, or integration of the absorption may lead to measurable differences in the output. Still, the other metrics studied, namely refractive index and carrier-pair generation, are sufficient to confirm the structure was soundly recreated. With the model manually validated, a construction script was then written to allow for variation of model parameters with ease, in parametric sweeps. This script turns layer height and materials, spheroid height and radius, and pitch into model variables, which massively speeds up the parametric sweep process by allowing automatic variation of said parameters using Lumerical's built in sweep function.

### III. CONVERGENCE TESTING

Even though these models are idealized versions of the real system, numerical simulations like the ones performed in this work still contain numerical error. For this reason, it's important to be able to localize and quantify these error sources, and minimize them whilst keeping simulation times reasonable. This process is known as convergence testing. [10]

To ensure reliability while balancing computational efficiency, convergence testing was performed on key parameters: PML - Perfectly Matched Layers - (to minimize spurious reflections) and mesh settings (to resolve geometric and optical field variations). The PML layers were studied because in-

sufficient layers can cause artificial reflections, distorting field decay and absorption, leading to a major increase in simulation time. Mesh granularity, on the other hand, was analyzed because coarse meshing under-resolves critical regions (for example, the thin NiO layer or the edges of the spheroidal structures), while excessive refinement unnecessarily increases runtime and computational load. For the mesh case, three alternatives were studied: the global mesh, and localized meshes refined in the Z and in the XY directions.

In order to quantify the level of convergence, sweeps across the aforementioned parameters were performed, while evaluating the short circuit current  $J_{sc}$ . For single-point metrics, the difference with the results of the previous step can be given by [10]:

$$\Delta\sigma(i) = \sqrt{\frac{\int(\sigma_i(\lambda) - \sigma_{i-1}(\lambda))^2 d\lambda}{\int \sigma_i(\lambda)^2 d\lambda}} \quad (5)$$

But, since  $J_{sc}$  is already an integration over wavelength, the integrations can be dropped, leaving us with:

$$\text{Relative Error} = \left| \frac{J_{sc}^{(i)} - J_{sc}^{(i-1)}}{J_{sc}^{(i-1)}} \right| \times 100\% \quad (6)$$

The relative error for all four sweeps was plotted in figure 5, both in percentage and in absolute value.

Starting with the PML, we can see that the percentage error introduced by this parameter is near zero. Additionally, increasing the amount of PML has close to no impact on simulation time, and, in scenarios where a small number of PML isn't enough to fully dissipate the light that wasn't absorbed, having a smaller number of PML can actually greatly increase it. For this reason, the PML parameter was usually kept at around 20 across simulations.

Defining the mesh locally across the Z direction also generated a very small variation in the results, especially when taking into account the increase in simulation time and computational resources. The local mesh across the XY directions, on the other hand, showed a near 1% variation in its first iteration (from 4 to 5), and as such, a local XY mesh with a refractive index of 5 was placed on top of the ITO spheroidal structures, to improve the initial interface between the light and the cell.

Finally, we can see that the difference in results when varying the global mesh falls under 1% when going from 2 to 3, so a global mesh of 2 should be enough to obtain good results.

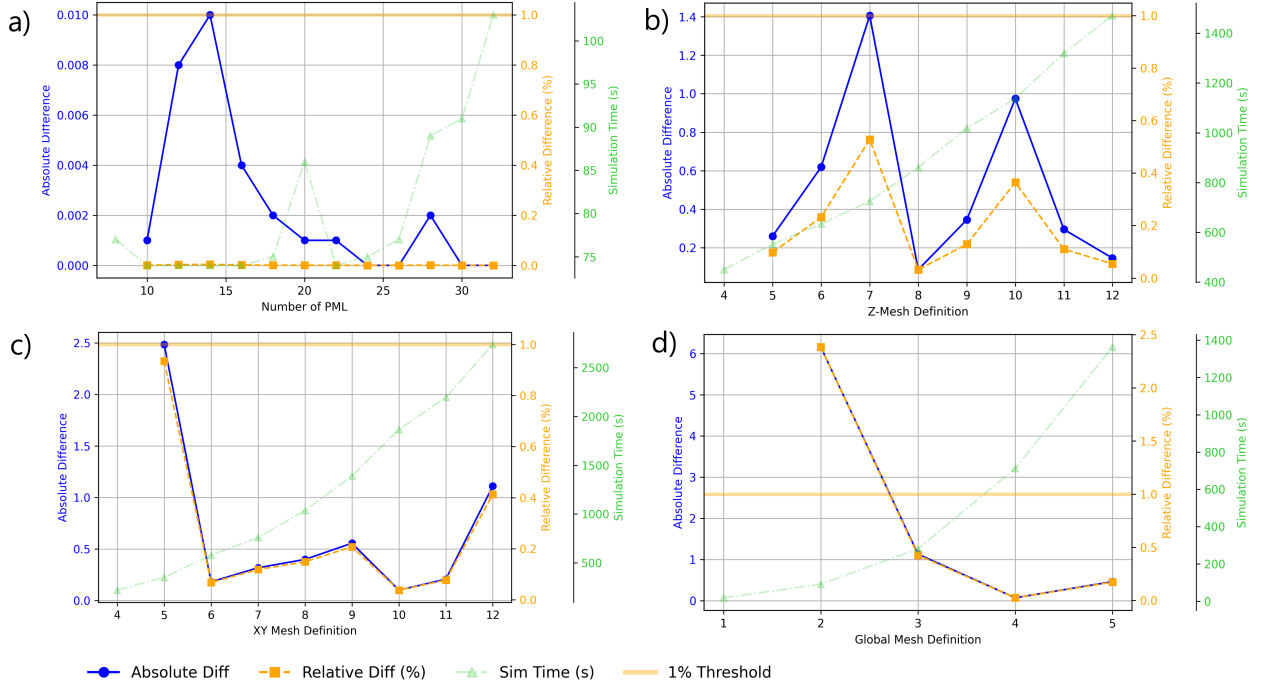


Figure 5: Convergence testing results, for a) - PML, b) - Local Z-Mesh definition, c) - Local XY-Mesh Definition and d) - Global Mesh definition.

#### IV. PARTICLE SWARM OPTIMIZATION

To find the best configuration for the AM0 cell nanopattern, a Particle Swarm Optimization (PSO) algorithm was used.

PSO is a stochastic metaheuristic based on the population, which is inspired by the social behavior of organisms such as bird flocks or fish schools [11]. It has been widely applied to the design of nanophotonics due to its ability to efficiently explore complicated, high-dimensional, and non-differentiable parameter spaces [12].

In the PSO algorithm, an array of  $N$  particles is initialized with random position vectors  $\mathbf{x}_i$  and velocity vectors  $\mathbf{v}_i$  in the parameter space. Each particle computes the figure of merit (FOM), which in this case is the short-circuit current,  $J_{SC}$ , at its present position and remembers the best solution it has ever encountered, which is denoted  $\mathbf{p}_i$ . At the same time, the best-known position of all particles is globally stored as  $\mathbf{g}$ .

At each iteration, particle velocities are updated by a combination of inertia, cognitive, and social terms. The update rule is given by [13]:

$$\mathbf{v}_t = \mathbf{v}_{t-1} + c_1 \eta_1 (\mathbf{p}_{t-1} - \mathbf{x}_{t-1}) + c_2 \eta_2 (\mathbf{g}_{t-1} - \mathbf{x}_{t-1}) + (\omega - 1) \mathbf{v}_{t-1} \quad (7)$$

where  $c_1$  and  $c_2$  are learning coefficients determined by the user,  $\eta_1$  and  $\eta_2$  are random numbers uniformly distributed in  $[0, 1]$ , and  $\omega$  is the inertia weight for momentum.

Then the position of every particle is updated:

$$\mathbf{x}_t = \mathbf{x}_{t-1} + \mathbf{v}_t. \quad (8)$$

This procedure is iterated over a specified number of generations, in this case 500, or until convergence criteria are reached.

PSO is commonly used for optimizing structural parameters such as nanohole radius, period, or layer thickness of optoelectronic devices. The fact that PSO is derivative-free makes it suitable for simulations where the gradient information is unavailable or unreliable [13].

Through the use of PSO to maximize  $J_{PH}$  or absorption in the perovskite layer, one can iteratively converge to optimum nanophotonic geometries in the absence of an explicit model for the physical response surface.

Since this optimization algorithm has some random components, two PSOs were ran in this work,

to guarantee the soundness of the results. Both optimizations converged to around the same structural values, as can be seen on Table III.

Table III: Results of both PSO runs.

	1st Run	2nd Run
$p$ ( $\mu m$ )	0.5133	0.5133
$R_z$ ( $\mu m$ )	0.5888	0.5887
$R$ ( $\mu m$ )	0.2	0.2

Something of note here is that for both runs, the value set as the minimum for  $R$  was deemed most efficient. This suggests that there might be a value of  $R$  for which  $J_{PH}$  is higher and that wasn't captured in the PSO algorithm's range. This will be considered in and discussed further in Section VII.

Nonetheless, and as was expected, these optimized parameters perform better under AM0 than the ones that resulted from the optimizations performed in [5], boasting a 1.62% increase in efficiency. It is also possible to compare the  $J_{PH}$  under both spectral conditions for the optimized structures, taking the aforementioned  $26.8mA/cm^2$  up to around  $31.8mA/cm^2$ , marking a 18.6% increase. Naturally, this was to be expected, since integrating the AM0 spectrum yields a higher integrated power, so these values must be interpreted along with the difference in integrated power of the two spectra in the wavelength range simulated. For the AM1.5G spectrum, this value is 739.3W and for the AM0 spectrum it is 931.4W, representing a 20.62% increase.

Additionally, it also significantly outperformed the planar cell under AM0, which had a  $J_{PH}$  of  $26.6mA/cm^2$ , meaning the nano-structures **improved efficiency by 19.55%**. The charge carrier generation density can be seen in figure 6.

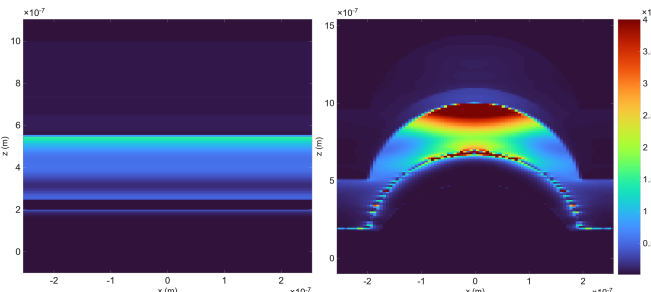


Figure 6: Rate of electron-hole pair generation for the nanopatterned cell and for the planar cell structures, in an xz cross-section at  $y=0$ ; under AM0.

## V. PARAMETRIC ANALYSIS

Having determined the best cell geometries for the AM1.5G [5] and AM0 spectra, we next parametrically vary the structure parameters around the reference points in order to determine their impact upon current generation. This is relevant because certain geometrical shapes can have the effect of producing strong local maxima in performance. For such cases, small deviations from the optimal geometry due to fabrication tolerances can produce large losses in efficiency. Thus, these wider, more solid performance peaks of the designs are to be utilized in place of narrow, high-sensitivity optima designs. Furthermore, the impact of varying layer thicknesses will be investigated to highlight the limitations of the optical-only simulations without taking electrical factors into account.

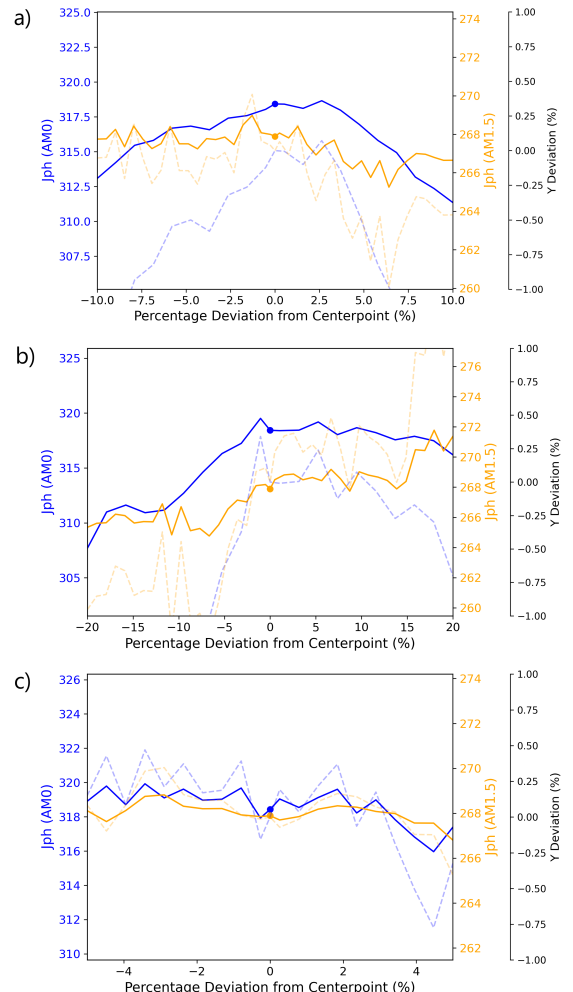


Figure 7: Parametric sweeps for the pitch (a), radius (b) and height (c) as a deviation from the centerpoint.

Firstly, from the AM1.5G structure analysis, it's

possible to see that often the  $J_{ph}$  values from points in the vicinity of the original optimized parameters exceed the reference point of the source material. This is unexpected since a properly converged optimization should have a local maximum with all of the configurations in the nearby region having worse performance. But this difference is most likely not due to a failure of optimization but due to differences in simulation environment and numerical implementation. As discussed before, differences in the way refractive index data is interpolated, absorption is integrated, or the mesh resolves field distributions at material boundaries can all impact the final current density. Therefore, although structural parameters were reproduced, performance variations observed in the results indicate the sensitivity of optical optimization to numerical setup. The variations are, however, less than 0.50% for pitch and height, and just over 1% for radius.

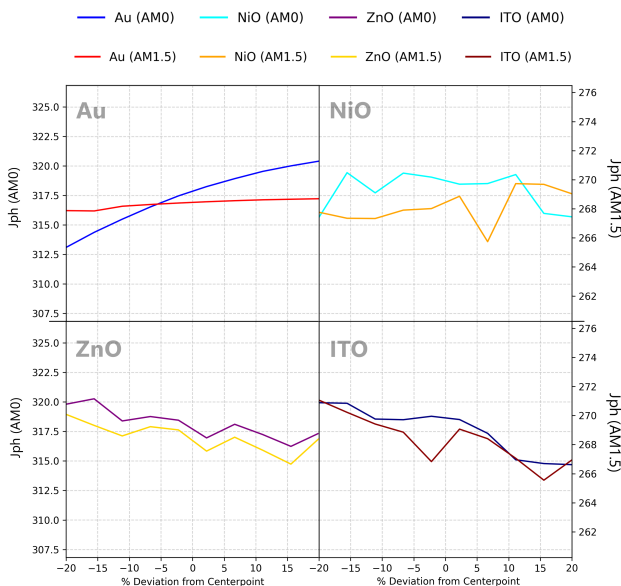


Figure 8: Parametric sweeps for the layer thicknesses of all materials except the active layer. These represented a 40% deviation from tabled values.

In the case of the AM0 results, where the optimization was performed under the exact same conditions as the parametric sweep, we can see that our percent deviations from the center-point are much smaller, especially for pitch and radius. Here we can also verify the presence of the aforementioned possible high at radii lower than  $2\mu m$  that weren't captured in the PSO. This deviation is small enough that it can be ignored without impacting the cell's performance in any major way, but, if required, an-

other PSO could be ran with increased ranges for the spacial parameters. Even taking this into account, no simulation surpassed the center-points by more than 0.50%, this time the biggest deviations being found in the heigh sweep.

Lastly, the layer thickness sweeps were performed (figure 8), from an optical optimization standpoint. This could be useful in case there were any big peaks around the points studied that could greatly enhance optical performance without hindering electrical performance or fabrication processes. A big take-away from this type of verification is that optical effects aren't the only things that affect cell efficiency. For example, from a purely optical standpoint, eliminating the NiO layer completely would yield the best results, but this would leave the cell without an ETL, and therefore lower its overall efficiency. This is also the reason these parameters weren't included in the PSO. Apart from that, we can see that increasing the size of the gold back contact would increase optical efficiency, most likely due to increased reflection back into the cell and thus better photon recycling. On the other hand, all three oxide layers (ITO, ZnO, and NiO) show decreased optical performance with increasing thickness, likely due to parasitic absorption or interference losses.

## VI. POLARIZATION

Comprehension of the polarization effect and incidence angle of light is required in reasonably evaluating the true performance of solar cells under practical conditions. Sunlight never approaches the cell surface at right angles in real applications, and sunlight is also never completely polarized. Variations of incidence angles throughout the day and throughout seasons, as well as polarization variations through atmospheric scattering or through optical elements (i.e., concentrators, glazing glass), can significantly influence light absorption and electrical energy conversion. It is therefore desirable to be aware of these effects while designing highly efficient structures for various illumination conditions, especially under non-stationary conditions such as in satellites or mobile platforms.

Firstly, in figure 9, we can see that the  $J_{PH}$  starts dropping at an incidence angle of the light wave off around  $35^\circ$ . This drop-off happens earlier than in most reference material [14], [15], where the drop-off angle seems to be consistent at around  $55^\circ$  for cells with various types of light trapping structures.

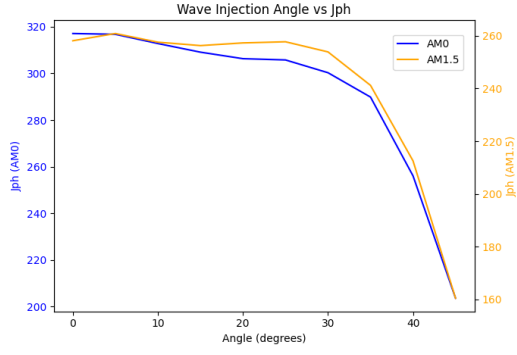


Figure 9: Variations in  $J_{PH}$  for different angles of light incision.

A possible reason is that the specific geometry of the nanostructure employed in this work is very sensitive to wavefront direction. Coupling of light into resonant modes or guided trajectories might degrade faster with off-normal incidence in this structure, and hence absorption in the active layer at shallower angles will be decreased. However, effects due to simulation cannot be ruled out. The earlier drop-off can also potentially be caused by mesh resolution limits or partially normalized sources against angular projection. Additional careful convergence analysis or experimental observations would be required to fully conclude whether the effect is physical or numerical in nature.

As for the polarization effects on the cell, figure 10 shows that  $J_{PH}$  has a very small sinusoidal dependence on the polarization angle, with a peak to peak variation of only 0.56% for AM0 and 0.40% for AM1.5G. Under unpolarized or randomly polarized light, this effect will not be present, since this sinusoidal effect averages out. Thus, the cell design can be considered effectively polarization-independent for real-world solar illumination.

Yet, under controlled conditions in a laboratory setting and with a polarized light source, like a laser, this limited dependence might be quantifiable. Under such setups, the polarization of the incident light couples to the structure along fixed directions relative to the simulation ones, and even tiny numerical or mesh anisotropies will produce weak but observable polarization sensitivity. Such phenomena are not intrinsic to the honeycomb geometry itself, which is symmetric, but rather appear as an artifact of the relative orientation of the electric field vector to the discretization grid and simulation domain. These small discrepancies are thus expected and do not represent any significant polarization-dependent loss in practical application [16].

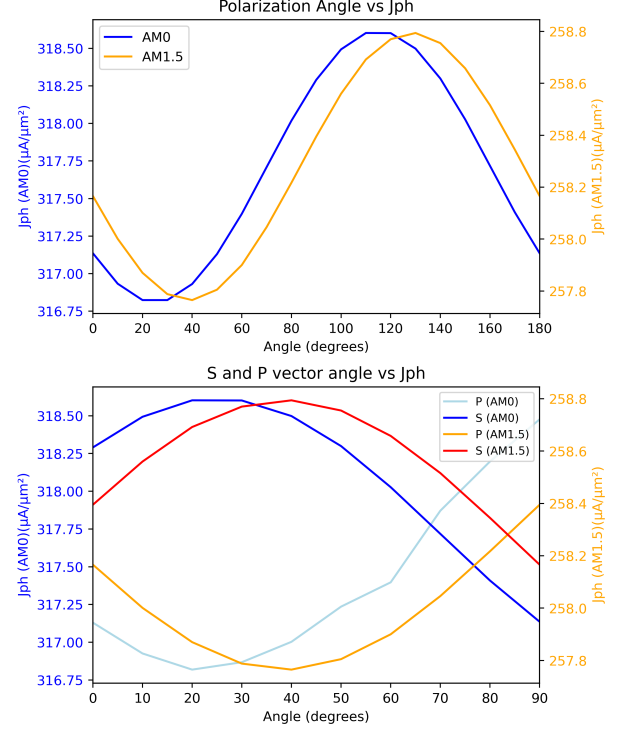


Figure 10: Variations in  $J_{PH}$  under different polarization angles.

## VII. CONCLUSIONS AND DISCUSSION

This study successfully demonstrated the optical optimization of nanopatterned  $\text{CH}_3\text{NH}_3\text{PbI}_3$  perovskite solar cells using Ansys Lumerical FDTD simulations.

Convergence testing was conducted, which confirmed that numerical parameters such as PML thickness and mesh resolution introduce negligible error when correctly set and under normal conditions.

A particle swarm optimization algorithm was used to find the nanostructure configuration that maximized light absorption in the active layer, leading to an 19.55% increase in  $J_{ph}$  under AM0. These results highlight the effectiveness of nanopatterning in enhancing light trapping without increasing material consumption.

Parametric sweeps around the optimum geometry exhibited low sensitivity to fabrication variations, demonstrating that the optimized designs are not inappropriately fragile. Sweeps around a literature reference structure exhibited small discrepancies attributable to simulation environment and numerical interpolation differences, highlighting the importance of internal consistency in simulation-based optimization chains. The study also explored the effect

of layer thicknesses on performance from an optical standpoint. It was found that while thinner layers can enhance light absorption, they will interfere with electrical operation.

Finally, polarization analysis showed that the cell has roughly constant performance for various incident light polarizations. The design is effectively polarization-independent under solar conditions and is at most weakly sinusoidally varying for idealized laboratory conditions. Studying the cell's efficiency under different light incidence angles shows that this cell structure might be more dependent on this factor than other similar cell structures.

In summary, this study shows how advanced optical modeling and algorithmic optimization can guide the design of ultra-efficient perovskite solar cells with important implications for terrestrial and space-based photovoltaics. The methodology and results provide a solid foundation for future co-optimization with electrical modeling and experimental validation.

## VIII. FUTURE WORK

Parts of this study, like the parametric variation of the layer thicknesses or the incidence angle variation, proved that the optical optimization is far from the last step of cell design. Other aspects must be taken into account, like fabrication techniques or electrical efficiency. This latter one is extremely significant, and, as such, further analysis of charge carrier movement inside the optimized cell is recommended. This can and has been done using FEM analysis techniques [6].

The consideration of optical performance is an even smaller percentage of space photovoltaics. This field has many more parameters to be taken into account, such as resistance of materials to high radiation, thermal cycling at extreme temperatures, mechanical endurance in launch, and vacuum and microgravity stability over long periods of time. The performance of encapsulation layers, resistance to UV degradation, and atomic oxygen erosion are the important parameters. Therefore, while maximizing light absorption is necessary, material and architectural choice must ultimately be determined by their suitability to the extreme space environment. This guides the necessity for a multidisciplinary design approach addressing thermal management, structural integrity, and radiation blocking, as well as optoelectronic performance.

Finally and perhaps more importantly, it is nec-

essary to confirm these results experimentally in the lab, not only to confirm trends observed in simulation but also to uncover secondary effects that will not be apparent with pure optical modeling, e.g., surface roughness, non-ideal interfaces, and layer thickness or material property deviations.

## REFERENCES

- [1] L. Andreani, A. Bozzola, P. Kowalczewski, M. Liscidini, and L. Redorici, "Silicon solar cells: Toward the efficiency limits", *ADVANCES IN PHYSICS: X*, vol. 4, pp. 1 548 305–1 548 329, 2019.
- [2] F. Cao, L. Bian, and L. Li, "Perovskite solar cells with high-efficiency exceeding 25%: A review", *Energy Materials and Devices*, vol. 2, pp. 9 370 018–9 370 038, 2023.
- [3] G. Niu, X. Guo, and L. Wang, "Review of recent progress in chemical stability of perovskite solar cells", *Journal of Materials Chemistry A*, vol. 3, pp. 8970–8980, 2015.
- [4] M. Ren, X. Qian, Y. Che, T. Wang, and Y. Zhao, "Potential lead toxicity and leakage issues on lead halide perovskite photovoltaics", *Journal of Hazardous Materials*, vol. 426, pp. 127 848–127 861, 2022.
- [5] S. Haque and M. Alexandre, "Supplementary material - photonic-structured perovskite solar cells: Detailed optoelectronic analysis", *ACS Photonics*, vol. 9, pp. 2408–2421, 2022.
- [6] S. Haque and M. Alexandre, "Photonic-structured perovskite solar cells: Detailed optoelectronic analysis", *ACS Photonics*, vol. 9, pp. 2408–2421, 2022.
- [7] A. Inc. "Ansyst numerical fdtd". (2024), [Online]. Available: <https://www.ansys.com/products/optics/fdtd> (visited on 06/16/2025).
- [8] A. Inc. "Finite-difference time-domain (fdtd) solver introduction". (2024), [Online]. Available: <https://optics.ansys.com/hc/en-us/articles/360034914633-Finite-Difference-Time-Domain-FDTD-solver-introduction> (visited on 06/16/2025).
- [9] PV Education. "Standard solar spectra". (n.d.), [Online]. Available: <https://www.pveducation.org/pvcdrom/appendices/standard-solar-spectra> (visited on 06/16/2025).
- [10] A. Optics. "Convergence testing process for fdtd simulations". (), [Online]. Available: <https://optics.ansys.com/hc/en-us/articles/360034915833-Convergence-testing-process-for-FDTD-simulations> (visited on 06/06/2025).
- [11] J. Kennedy and R. Eberhart, "Particle swarm optimization", *Proceedings of ICNN'95 - International Conference on Neural Networks*, vol. 4, pp. 1942–1948, 1995.
- [12] A. Rodriguez, P. Bermel, and S. Fan, "Design of photonic nanostructures for solar cells using coupled optical and electrical modeling", *Optics Express*, vol. 25, no. 8, pp. 9405–9417, 2017.
- [13] A. Optics. "Optimization utility". (), [Online]. Available: <https://optics.ansys.com/hc/en-us/articles/360034922953-Optimization-utility> (visited on 06/16/2025).
- [14] I. Geisemeyer, N. Tucher, B. Müller, et al., "Angle dependence of solar cells and modules: The role of cell texturization", *Proceedings of the IEEE International Conference on Photovoltaic Specialists (PVSC)*, pp. 1–6, 2017. doi: [10.1109/PVSC.2017.8366066](https://doi.org/10.1109/PVSC.2017.8366066).
- [15] C. Seshan, "Cell efficiency dependence on solar incidence angle", *Proceedings of the IEEE International Conference on Photovoltaic Specialists (PVSC)*, pp. 1–6, 2010. doi: [10.1109/PVSC.2010.5614472](https://doi.org/10.1109/PVSC.2010.5614472).
- [16] A. Hoblos, M. Suarez, B. Guichardaz, N. Courjal, M.-P. Bernal, and F. I. Baida, "Revealing photonic symmetry-protected modes (spm) by finite-difference-time-domain method", *arXiv*, 2019. [Online]. Available: <https://arxiv.org/abs/1912.11679>.